Time Development of Scour around a Cylinder in Simulated Tidal Currents.

McGovern, D. J.,[1,2] Ilic, S.[3] Folkard, A.M.,[4] McLelland, S. J.,[5] and Murphy, B. J.,[6]

[1] Lancaster Environment Centre, Lancaster University, Lancaster, LA1 4YQ, United Kingdom

[2] Corresponding author, current address: National University of Singapore, Department of Civil and Environmental Engineering, Hydraulic Engineering Laboratory, EW1-03-01A, 2 Engineering Drive 2, Singapore 117576. Email: david.j.mcgovern1@gmail.com

[3] Lancaster Environment Centre, Lancaster University, Lancaster, LA1 4YQ, United Kingdom

[4] Lancaster Environment Centre, Lancaster University, Lancaster, LA1 4YQ, United Kingdom

[5] Department of Geography, University of Hull, Hull, HU6 7RX, United Kingdom

[6] Department of Geography, University of Hull, Hull, HU6 7RX, United Kingdom

Abstract

A laboratory flume experiment was performed to investigate the time-development of scour around a vertical cylinder acting as a scaled model of an offshore wind turbine monopile in tidal currents. The tidal current was simulated by resolving each half cycle into three time-steps, between which flow velocity and depth were varied. Flow direction was reversed between half-cycles, which were otherwise identical. Between them, the three time-steps exhibited clear-water, transitional and live-bed conditions. The experiment was run over two full simulated tidal cycles. The scour hole formed tended to a symmetrical shape after two half-cycles and was both shallower and slower-developing than the scour hole in a unidirectional current test carried out in the same flume. This was due mainly to the variable rates of scour caused by the variable flow conditions within each half cycle, and to a lesser extent to the infilling of the scour hole when the current direction reversed. The lower scour depth recorded in tidal conditions implies that the amount of scour protection required may be less than previous studies suggest.

Subject Headings: Hydraulic models, Scour, Cylinders, Wind power, Sediment transport

Introduction

Offshore wind energy generation is a rapidly expanding sector of the renewable energy market, particularly in the UK (e.g. Wilson et al. 2010). Offshore wind turbine farms are popular because they are larger, have lower visual impact and are situated in higher wind speed environments than their onshore counterparts. A significant problem associated with their deployment is bed scour at the base of their monopile foundation structures. Flow modification by the monopile increases velocity and turbulence. The resulting amplification of bed shear stress can induce scour, causing large, steep-sided holes around the monopiles. This can reduce their stability and longevity (e.g. Breusers and Raudkivi 1991; Melville and Coleman 2000). It can also cause 'free-spanning' of cables attached to the monopile, i.e. exposure from their original buried positions (e.g. Zaaijer and Van Der Tempel 2004; De Vos 2008).

There are numerous studies of scour around bridge piers in steady, unidirectional flow (e.g. Shen et al. 1969; Melville 1975; Ettema 1980; Raudkivi and Sutherland 1981; Melville and Sutherland 1988; Sheppard et al. 2004), because of its importance in rivers. These have often aimed to define empirical equations for predicting equilibrium scour depth (d_{sce}), the depth of the scour hole when flow modification by the structure no longer changes it significantly. Comprehensive reviews of this research can be found in Breusers et al. (1977), Hoffmans and Verheij (1997) and Melville and Coleman (2000).

Predicting scour in marine environments has the added complexity of unsteady flow. The action of waves, which generate short-lived currents, is reasonably well understood (e.g. Sumer et al. 1992; Sumer et al. 1992a; Sumer et al. 1997; Whitehouse 1998; Sumer and Fredsøe 1999; Sumer and Fredsøe 2001; Jensen et al. 2006; and De Vos 2008), but the effects of tidal flow are less understood. While the instantaneous structure of tidally-induced flow fields around a cylindrical obstacle is broadly analogous to that of unidirectional currents (Whitehouse 1998), variations in velocity and water depth during a tidal cycle may cause significant differences in scour patterns. An important parameter for quantifying these scour effects is the flow intensity U/U_c, where U is flow speed, and U_c is the critical flow speed for sediment motion. Flow intensity values can be used to distinguish between live-bed regimes ($U/U_c > 1$), where the flow is strong enough to move sediment regardless of the presence of the obstacle, and clear-water regimes ($U/U_c < 1$), where only its interaction with the obstacle causes sediment movement. These two regimes generate different scour hole time-developments and equilibrium depths (Figure 1). While uni-directional flow environments generally remain in one or other regime, tidal flows may pass between them within each tidal period. Thus, a different pattern of scour development from that of a steady unidirectional current may be expected.

Escarameia and May (1999) conducted a laboratory study of the time-development of scour depth around various structures including a vertical cylinder under reversing flow conditions. For a square, vertical cylinder flow speed and depth were varied independently. For a circular cylinder, a single test was performed in reversing currents of constant depth and speed. The results demonstrated a smaller equilibrium depth for scour than found under unidirectional flows due to infilling of the scour hole during flow reversal. It was also found that the maximum scour depth was reached for a live-bed state ($U/U_c > 1$), rather than a transitional state ($U/U_c = 1$) as is observed in unidirectional currents. In unidirectional currents, clear-water scour generates the greatest equilibrium scour depths, because there are no migrating bedforms which change the scour depth during live-bed conditions. During the reversing current experiments, Escarameia and May (1999) observed that live-bed flow generated the greatest scour depths because it nullified the effect of infilling of the scour hole when the current reversed direction. Their study also suggests that the generation of bedforms alters the velocity field when the current reverses. Jensen et al. (2006) and Margheritini et al. (2006) also investigated tidal scour around a vertical cylinder. Margheritini et al. (2006) reported a series of experiments to investigate tidal scour at a single vertical circular cylinder (a scaled offshore wind turbine monopile). They approximated tidal flow to a 'square' tide (i.e. alternating equal and opposite constant velocity and depth flows, simplifying the typically sinusoidal nature of tidal variations, Figure 2), which resulted in permanently live-bed conditions. Jensen et al. (2006) found that the scour hole formed was symmetrical and had a larger eroded volume than the equivalent, asymmetrical unidirectional scour hole, although scour depth was found to be similar to the unidirectional case. These results are at odds with those of Escarameia and May (1999) who reported shallower scour holes in tidal currents.

Time development of scour in uni-directional flow conditions has been well studied (e.g. Hoffmans and Verheij, 1997). Sumer et al. (1992) and Melville and Chiew (1999) both derived empirical predictions of the time-scale for equilibrium depth in unidirectional flow conditions. Melville and Chiew (1999), working in purely clear-water conditions, defined this as the time after which scour depth increases by less than 5% in 24 hours. They found this to be

$$t_{e(days)} 30.89 \frac{D}{U}\left(\frac{U}{U_c} - 0.4\right)\left(\frac{h}{D}\right)^{0.25} \qquad \text{for } h/D \leq 6 \qquad (1)$$

where U/U_c is the flow intensity, D is cylinder diameter, and h is water depth. They also provided a prediction of the time evolution of scour depth:

$$d_{sc} = \exp\left(-0.03\left|\frac{U_c}{U}\ln\left(\frac{t}{t_e}\right)\right|^{1.6}\right) d_{sce} \qquad (2)$$

where d_{sce} is the equilibrium scour depth. The development of scour for live-bed conditions may be predicted using the method of Sumer et al. (1992):

$$d_{sc} = d_{sce}\left(1 - \exp\left(\frac{-t}{t_e}\right)\right) \qquad (3)$$

The term t_e was determined empirically as

$$t_e = \frac{D^2}{(g(s-1)d^3)^{\frac{1}{2}}} \frac{1}{2000} \frac{h}{D}\left(\frac{{u_*}^2}{g(s-1)d}\right)^{-2.2} \qquad (4)$$

where s is the specific gravity of the sediment and $u_* = \sqrt{(\tau_b/\rho_w)}$ the shear velocity, d = mean sediment particle diameter, where τ_b is the bed shear stress - calculated using the TKE method (e.g. Kim et al. 2000) and ρ_w is the density of water.

However, there remains significant uncertainty regarding the development and equilibrium depth of scour holes around cylindrical obstacles, such as wind turbine monopiles, in tidal flows. The study reported here was carried out to address this. In particular, it explores the effects on scour hole development of simultaneous changes in flow depth and speed through the tidal cycle, thereby expanding on previous studies which have separated out speed and depth effects (Escarameia and May 1999) or idealized tidal flow using a square-wave pattern (Jensen et al. 2006).

Methods

A series of laboratory flume experiments was conducted in The Total Environment Simulator Tank at The Deep, Hull, U.K. Within the 16 m long, 6 m wide, re-circulating tank, a 1.2 m wide by 11 m long channel was constructed (Figures 3 and 4). Flow was driven in one direction by an electric pump housed under the flume, and in the other by nine submersible pumps. Control tests in undisturbed (no cylinder) conditions were taken to ensure that the opposing flows exhibited the same velocity profiles. A lattice screen conditioned the flow at the inlet to the flume. The monopile was simulated using a 0.2 m diameter PVC cylinder positioned with its centre at the flume mid-point (Figures 3 and 4). The blockage ratio of 1:6 was within the limits advised by Whitehouse, (1998) and therefore blockage effects were assumed insignificant. The influence of the side walls is also considered negligible, since the lateral limits of the scour holes formed remained > 20 cm away from both side walls. The flume bed was composed of sand with a median diameter d_{50} = 0.135mm d_{10} = 0.088mm and d_{90} = 0.211mm and density ρ = 2.65 g/cm^3. Its natural angle of repose was ≈ 45˚, and it was of uniform grading according to the manufacturers specifications. The

flume was filled with fresh water of density = 1000 kg/m^3 and salinity < 0.1 ‰. No direct temperature measurements were taken but, as this was mains water, the temperature was likely in the range of 5 – 15°C, depending on ambient temperatures at the time. It was assumed that using freshwater would have negligible effect on density and viscosity of the water in comparison with sea water as long as the flow conditions were turbulent (see discussion of scaling below). The flume bed was built-up using bricks to give a sediment depth of 0.1 m except in the central section of the flume channel (1 m up and downstream of the cylinder) which was filled with sediment to a thickness of 0.4 m.

Runs of the experiment were carried out under both unidirectional and reversing flow conditions. The reversing current was designed to approximate a sinusoidal, non-progressive (standing wave) tide, each tidal half cycle being approximated in three time-steps, as illustrated in Figure 5. The flow speed and depth in each time step were derived from a prototype tide, based on measurements from the British Oceanographic Data Centre taken in Liverpool Bay, UK, the location of several existing and proposed offshore wind farms. A sample of this data is shown in Figure 6. The choice of water depth is based on field data from the Rhyl Flats wind farm of recorded lowest annual tide water depths around individual monopiles. Reversing pump capacity limits necessitated a reduction of flow depth to achieve the desired flow speeds. Therefore, it is noted that the water depths used in this study are lower than would generally be found in the field, though not implausible. A detailed discussion of the scaling from this prototype data to the model, including the choice of water depth is given by McGovern (2011). The first prototype tidal half-cycle was constructed by taking mean values of flow velocity for each third of the corresponding half-cycle in the Liverpool Bay data. The subsequent half-cycle was constructed by assuming tidal symmetry, and the flow depth calculated for each time-step from the mean of the measured tidal ranges associated with the velocity data. The length scale l of the experimental model (m) was 1/20th that of the prototype (p) data. The velocity and time scaling between the prototype and model was determined by requiring Froude number $F = U/(gh)^{1/2}$ similitude. The changes in the free surface and resulting flow in the vicinity of the cylinder can be characterised by F. Larger values of F are associated with a larger difference between the surface elevation in front and side edge of the cylinder resulting the induced pressure gradient driving a strong down flow with a very strong component of flow velocity in the radial direction (Roulund et al. 2005). Smaller F is associated with flow conditions for which the 'head' difference is too small to cause any significant flow in the radial direction. F similarity, therefore, ensures similitude of flow conditions around the cylinder. The scale relationships are given in Equations 5, 6 and 7 where L, V and T are the length, velocity and time scales respectively. The ratio of prototype to model time scale is $\sqrt{20} = 4.47$. This gives a model half-cycle of 81 minutes, therefore each model time step is 27 minutes. Reynolds number $R = Uh/v$ was greater than 10^4, and thus fully turbulent, in both model and prototype (Hughes, 1993).

$$L_p = lL_m \quad (5)$$

$$V_p = \sqrt{l}V_m \quad (6)$$

$$T_p = \sqrt{l}T_m \quad (7)$$

Due to the well-known difficulty of geometrically scaling sediment particle size (e.g. Ettema et al. 1998), the flow speeds used were raised above those given by Froude scaling to attain similitude in the flow intensity (U/U_c), resulting in the flow speeds given in Table 1. Such values lead to relatively large current speeds when scaled up to the prototype. U_c was calculated following Melville (1997). There remains a scale effect in the cylinder boundary layer, which is laminar in the model but turbulent in the prototype. The nature of the boundary layer is related to the cylinder Reynolds number ($R_D = UD/v$) which is approximately 10^4 in the model but 10^6 in the prototype. The main effect of this is to alter the lateral location of boundary layer separation on the cylinder. However, it is noted that the vortex shedding this separation causes is not a primary mechanism of sediment entrainment. Rather, its main effect on the sediment is to transport it downstream (for example see Melville 1977 and Breusers et al. 1977). Therefore, R dissimilitude is not likely to have a significant effect on the local scouring process. Moreover, from Figure 1.9 of Sumer and Fredsøe (1997) which shows the Strouhal number ($St = f_v/D$, where f_v = the frequency of vortex shedding) as a function of R_D, the rate of vortex shedding at prototype R_D (~ 0.2 for the transition and live-bed conditions, and ~ 0.1 for the clear-water test) is similar to rate for the model (in which R_D ~ 0.2 throughout). Therefore, the separation regimes of both the model and prototype exhibit similar St values, suggesting a similar rate of sediment transport out of the system. Hence, it is assumed

that the scale effect in the cylinder boundary layer will be minimal.

The reversing current test was simulated for two full tidal cycles, a total of 12 time steps, referred to as TS1-TS12 (so the first half cycle is made up of TS 1-3 etc.). The 'upstream' and 'downstream' sides of the cylinder change with flow direction. During 'positive' flow, the 'A' side is upstream of the cylinder and the 'B' side downstream, and *vice versa* during 'negative' flow. A rectilinear coordinate system is used with x denoting longitudinal position (positive on the B side, x=0 at the cylinder centre) and y denoting lateral position (positive to the right when looking towards the A side, y=0 at the cylinder centre). The x and y positions are normalised by the cylinder diameter D, such that $x' = x/D$ and $y' = y/D$. The plane $y' = 0$ is referred to as the 'centre-plane'. The parts of the centre-plane on the 'A' and 'B' sides are referred to as the 'A plane' and 'B plane' respectively.

The unidirectional test was run as a control. This was performed under live-bed conditions, because they result in the fastest rate of scour, and thus are hypothesized to be the flow conditions that cause most scouring in the reversing current situation (Escarameia and May 1999). While the velocity U = 0.31m/s was kept the same as in the reversing live-bed time-step, due to logistical difficulties, water depth was 5cm greater (h = 0.25 m). Despite this, the use of this unidirectional data for comparison is valid, within certain limits. Firstly, at low F numbers such as those in this experiment (F = 0.22 for the unidirectional and live bed tests), the flow around the cylinder is not significantly influenced by h/D (Roulund et al 2005). Furthermore, Hoffmans and Verheij (1997) argue that flow depth only has a direct effect on scour when h/D < 1. In the present experiments, h/D = 1.25 in the unidirectional test and h/D = 1 in the live-bed time-steps of the reversing flow tests, thus in both conditions, water depth was expected to have little effect on scour development. These h/D values lie in an 'intermediate' range where the influence of flow depth on scour depth is only felt when the surface roller interacts with the horseshoe vortex (Melville 1997). Hence, the decreased flow depth in the reversing current tests may reduce the scour depth slightly. To quantify the potential difference in scour depths, maximum scour depths were calculated using a scour prediction equation. Following Johnson (1995), the most suitable such equation for transition, live-bed and clear-water conditions is the CSU equation (HEC-18 1993)

$$d_{sce} = 2K_1K_2K_3hF^{0.43}\left(\frac{D}{h}\right)^{0.65} \quad (8)$$

where K_1-K_3 are correction factors for, respectively, cylinder nose shape (1 for circular cylinders), angle of attack of flow (1 for circular cylinders), and bed condition (1.1 for these tests). The maximum predicted scour depths are 0.23m for h = 0.2m, and 0.25m for h = 0.25m. Thus, the effect of the different water depths on the scour depth is <10%. Therefore, comparison between the uni-directional and reversing current test scour depths is made within these limits.

Velocity profiles were measured 3 m away from the cylinder in both longitudinal directions, using Acoustic Doppler Velocimeters (ADVs), to ensure that velocity profiles were well-developed at both ends of the experiment (McGovern, 2011). Time-series of bed elevation around the cylinder were collected with a Seatek Ultrasonic Ranging System (URS). The URS derives bed elevation from measurements of the travel time of acoustic 'pings' from transducers to the bed and back. In this deployment, 12 transducers were positioned around the circumference of the pile at 0º, 90º, 180º and 270º from the centre-plane, and at radial intervals of 10 cm, beginning at 6.5 cm from the pile's surface (Figure 8). Each recorded bed elevation measurement was the average of measurements from 20 'pings' made over 1 second, with the highest and lowest three readings removed. Time-series records were collected at all positions except on the downstream side (either the 0º or 180º position, Figure 8) due to the large amount of suspended sediment present in this region during tests, which interfered with the acoustic signal. Only measurements from the start and end of each element of the tidal cycle are presented in the downstream planes, taken in still-water conditions.

Full bed profiles on either side of the cylinder were made at the end of each full test using a Leica Disto laser distance measurer. This was mounted on a rig that allowed sampling from x' = 6.75 to −6.75 and y' = 2 to –2 on both sides of the cylinder.

Results and Discussion

Smooth Cylinder, Reversing Current Test

Figure 8a-c shows the time development of scour in the first half cycle, TS1-TS3. Scour begins first at the sides of the cylinder, eventually attaining depths of 0.12D and 0.165D in the 90° and 270° planes respectively. This is consistent with the location of greatest bed shear stress amplification around the cylinder's circumference recorded in rigid bed tests (McGovern et al. 2009). In these tests, bed shear stress was calculated from velocity profiles using the TKE method:

$$\tau_b = C_1[0.5\rho(\overline{u"^2} + \overline{v"^2} + \overline{w"^2})] \quad (9)$$

where C_1 is a constant of proportionality, which is given the value 0.19, following Soulsby, (1986) and Kim et al. (2000).

In the centre-plane on the A side, scour is recorded after approximately 20 minutes at $x' = 0.325$, as the hole gradually expands upstream, to a depth of 0.04D. Downstream from the pile (B), there is sediment deposition, which is greatest near the cylinder ($x' = 0.095$D).

The rate of scour near the cylinder ($x' \approx 0.325$) increases significantly during live-bed conditions (TS2, figure 8b) remaining greatest in the lateral planes. There is evidence of deposition in the 270° plane further away from the cylinder ($y' = 1.325$). This may be attributed to the passage of ripples which were observed forming all around the cylinder, and were present throughout the remainder of the test (Figure 9). Along the centre-plane, scour is confined to $0.825 < x' < 0$ upstream from the cylinder and reaches a maximum depth of 0.195D. Downstream from the cylinder there is scour present for $x' < 0.825$ and reaches a maximum of 0.26D at $x' \approx 0.325$.

During TS3, the changes in scour depth were negligible. Scour in the lateral planes developed asymmetrically, which was unexpected. There are several possible reasons for this: heterogeneity in the approaching flow, non-uniform sediment distribution, asymmetry in bed-form development, or natural asymmetry in scour hole development.

Figure 10a-c shows scour hole development during TS4-6 in which the current direction is reversed, so the A and B sides become downstream and upstream respectively. As in TS3, TS4 shows negligible change in scour depth in the centre-plane.

During TS5, the rate of scour is similar on both sides of the cylinder. Scour in the A plane is delayed particularly at $x' = 0.325$ where, after five minutes, the scour depth has *decreased* by ~0.025D (Figure 10b), before increasing to 0.375D. Deposition in the B plane at $x' = 1.325$ increases to 0.09D. This is due to the large increase in scouring on the upstream side resulting in significantly more suspended sediment in the wake for TS5 which is deposited at this location.

The downstream (A) side scour depth increases significantly to 0.08 m, and extends beyond $x' = 1.325$. During the sixth time step (TS6) the scour hole exhibits the same asymmetrical, elongated shape, with a shallower slope downstream as at the end of time step 3 (TS3), though elongation develops in the opposite direction. This is in agreement with Margheritini et al. (2006), who observed the scour hole changing alignment in response to different flow directions. The end of TS6 is the end of the first tidal cycle and maximum scour depth is approximately equal in both along- and across-flow directions (0.48D and 0.455D in the 90° and 270° planes, 0.41D and 0.385D on the A and B sides of the centre-plane, respectively).

Figure 11a-c presents results from the third half-cycle where flow direction is positive. Most of the scouring in this half cycle occurs during TS8. Maximum scour depth at the end of TS9 and TS10 is 0.535D in the lateral planes and 0.46D in the centre-plane. The depositional mound in the B plane is reduced as the scour hole widens, most significantly during transitional (TS7) and live-bed conditions (TS8). By the end

of the clear-water condition in TS9, scour has extended to $x' = 1.325$ in the B plane, meaning less deposition than scour here. In the A plane, the slope of the scour hole remains approximately constant during TS7, but in TS8 there is a steepening of the slope between $x' = 0.325$ and 0.825, indicating a greater rate of scour closer to the cylinder than further out. By the end of this half-cycle, the scour has become more symmetrical.

During TS10-12, the scour depth increases to 0.505D, 0.555D, 0.495D and 0.52D in the 90°, 270°, A and B planes, respectively (Figure 12a-c). Relative to the previous half-cycles, the changes are small, indicating that scour depth is approaching equilibrium. The majority of scouring again occurs during the mid-tide live bed condition.

Time-Development of Scour in Reversing Flow

Figure 13 shows the time development of scour in the variable, reversing flow test at the probes closest to the cylinder in each plane (probes 1, 4, 7 and 10). The changes in h and U/U_c due to the different flow conditions of each time-step appear to be the main factors influencing the scour development with the clear-water, live-bed and transitional time steps exhibiting different rates of scour. It is often stated that the scour depth will reduce under reversed flow (e.g. Hoffmans and Verheij 1997; Escarameia and May 1999), due to infilling. Figure 13 shows that infilling does take place during some periods of flow reversal (e.g. TS4 and TS10). Observations during the experiments indicated that infilling occurred through slumping of sediment from the scour hole edge to the middle, and via small vertical vortices forming on the leading edge of the scour hole carrying small amounts of sediment into it. Infilling is clear at the start of live-bed conditions in TS5 (shown as a decrease in scour depth for the 5 minute measurement) and transitional conditions in TS7. The flow during clear-water time-steps (TS4 and 10) is too weak to generate significant scour or infilling. Infilling also occurs long after flow reversal in the 90° plane throughout TS9-12. However, infilling is quickly replaced by scouring during these time-steps, resulting in a net increase in scour depth. These observations imply that the effect of infilling on scour time-development is both a delay to the onset of scour and a reduction in scour depth.

The rate of measured scour due to the variable reversing flow decreases with time (Figure 13). The average scour depth at all four probes increased by approximately 26% between the end of the first and second half cycles. This reduced to approximately 9% between the second and third half-cycles, and approximately 5% between the third and fourth half-cycles. Equilibrium, as defined by Melville and Chiew (1999), is achieved when there is <5% increase in scour depth over 24 hours. Although this is not achieved by the end of the test, the reduction in scour rate indicated approaching equilibrium. The second cycle is a stabilisation stage, where the rate of scour decreases and the depth nears equilibrium (e.g. Hoffmans and Verheij 1997).

The best-fit exponential curve to the observed data is shown in Figure 14a, and extrapolated to equilibrium (equilibrium as defined by Melville and Chiew 1999, see above), which is reached at ≈ 5400 minutes (i.e. 90 hours), in Figure 14b. Clearly this extrapolation is only approximate due to the lack of data beyond 5.5 hours (the two full tidal cycles tested).

Comparison of Time-Development of Scour with Predictions and Unidirectional Data

The predictions of the time evolution of scour using (2) for the transition and clear-water time development and (3) for live-bed time development were compared with the experimental data. The predictions are based on the d_{sce} which, estimated by (8) was for the transition, live-bed and clear-water conditions of 0.9D, 0.95D and 1.15D respectively. The prediction method of Escarameia and May (1999) is not used here as it is not developed for the live-bed flow conditions or h/D ratios (> 1 in the high-tide condition) used in this test.

The time-development of scour at Probes 1, 4, 7 and 10 is plotted in Figure 15a together with these predictions. Figure 15b shows the curves predicted using same equations, but using the final measured depth (0.59D) as the equilibrium scour depth.

Figure 15a shows that the changes in current velocity, depth and direction influence the rate of scour. The

development of scour in the variable reversing test is less smooth than in the case of the unidirectional flow, and as predicted by (2) and (3), which do not capture the recorded unidirectional scour very well either. The maximum scour depth at the end of the variable reversing test was 0.59D (Figure 15a). This is well below the predicted equilibrium depths of 0.9D, 0.95D and 1.15D for the transition, clear-water and live-bed conditions respectively. The recorded maximum scour depth for the unidirectional test was 0.8D (Figure 15a) which is 25% greater than for the variable reversing current test (significantly more than the ≈10% effect of the deeper water). The unidirectional test was conducted for 2.7 hours, equivalent to half of the variable reversing test period (i.e. one full tidal cycle). These observations confirm previous findings that both a faster rate of scour (hence a faster time to equilibrium) and greater scour depth occurs in the live-bed unidirectional current than in the variable reversing current. This observation conflicts with the results Jensen et al. (2006) but is in general agreement with Escarameia and May (1999). These differences can be explained when the nature of the tidal simulations are considered. Jensen et al. (2006) employed a 'square tide' (Figure 2), which gave live-bed conditions with no changes in depth and velocity. As a result, their scour hole developed much faster than in our experiment. The present experiments employ a closer approximation to a sinusoidal tide (Figure 5) and are closer to Escarameia and May's (1999) experiment, which investigates the independent influence of changes in flow speed, direction and depth. This implies that the variability of tidal flow depth and velocity needs to be taken into account when predicting scour depth in tidal conditions. Furthermore, the significant underestimation of the scour development by (2) and (3) of the recorded unidirectional scour indicates that these equations which ought to be conservative for design purposes, require greater accuracy.

In Figure 15a, the scour depth for the transition flow regime (low-tide) predicted by (2) appears to overestimate the measured scour rate initially, while the measured depth remains significantly lower throughout. This is probably due to a combination of the probe location being 6.5 cm from the cylinder, a slower rate of scour, and perhaps a lower d_{sce} (as will be discussed in greater detail below). The predicted rate of scour using (2) and (3) matches the measured data in the first tidal cycle, though the individual measured rates during live-bed stages (TS2 and TS5) are larger. Overall, (2), which is for clear-water conditions, gives the best prediction of the measured time development of scour. The slower-than-predicted rate of scour development during the second tidal cycle indicates that the equilibrium depth may be smaller than those predicted and used in the models (see also below). While the clear-water curve provides the best prediction of the time-development, this does not necessarily indicate that the equilibrium scour depth is closer to the predicted clear-water value of 0.95D.

Figure 15b compares the measured and predicted time-development curves calculated using the measured maximum scour depth (0.59D). The clear-water, transition and live-bed time-development curves all underestimate the measured rate of scour. It is difficult to tell whether this is because the measured d_{sc} is not the equilibrium depth, but it clearly indicates that in order for these equations to predict the measured data well, the equilibrium depths used need to be larger. The poor fit of the predictions to the measured data also indicate that such equations, which are intended for unidirectional flow conditions, are inappropriate for tidal flow scour prediction.

Equilibrium Scour Depth under Variable Reversing Currents

The equilibrium scour depth in the variable reversing current test is lower than that in the unidirectional test, and those predicted by the models. The CSU equation (8) predicts an equilibrium scour depth of 1.15D. The extrapolation of the exponential curve fitted to the data in Figure 14 gives $d_{sce} < 0.6D$, indicating that equilibrium scour depth in these experimental conditions is significantly over-estimated by the predictions. The scour depth recorded by each probe may not be representative of the maximum scour depth, as this will likely occur closer to the cylinder than the location of the probes. Assuming that the slope angle remains constant to the edge of the cylinder, the maximum depths reached in each plane are given in Table 2. This assumption is conservative as the scour depth decreases very slightly closer to the cylinder's edge, due to the weaker turbulence and velocity in this region. This does not change the main observation that the calculated maximum depths in Table 2 are only slightly larger than the measured depths, and still significantly less than the predicted values. Thus, the measurements indicate that the equilibrium depth is significantly lower under a variable reversing current than a square tide current or a unidirectional current. This appears to be a combination of the different scour rate and maximum scour

potential associated with each time-step as well as the infilling that occurs during reversed flow, rather than infilling alone of scour under the reversed currents, as is often proposed (e.g. Hoffmans and Verheij 1997; Escarameia and May 1999). Consider the fact that in the unidirectional current, scoured sediment is being permanently removed downstream from the region around the monopile. There is a permanent loss of sediment from the monopile vicinity, whereas in the reversing flow more sediment is kept in the vicinity of the monopile, mainly in the form of a depositional mound and is thus available for infilling during reversed flow. This is particularly true when the reversed flow is of variable intensity as in tidal flow which, therefore, reduces the amount of time in which the most energetic flows such as live bed / transitional conditions can remove sediment completely from the monopile vicinity. Furthermore, the scouring potential during each half-cycle of the tide is significantly less than in the unidirectional flow over the same time period due to the inclusion of the clear-water regime that generates far less scour. This experiment also shows that, comparatively, the development of the scour hole in variable reversing currents is slower than in unidirectional currents. This reasoning, however, may only be valid for relatively low values of Shields parameter such as in these tests (θ = 0.044 – 0.11). In cases where Shields parameter is relatively large, the amount of sediment transport taking place in a single tidal half-cycle may become large enough to remove significantly more sediment from the monopile region. This would potentially decrease the amount of sediment available for back filling when the flow reverses. In such cases the scour depth may be influenced more by the Shields parameter rather than the duration of the half-cycle.

Of the two differences between the tidal and unidirectional flow conditions - changes in flow velocity and water depth – the latter appears less important here, as h/D falls below unity only in the transition (low-tide), therefore, there is little interaction between the surface roller and the downflow which causes scour (see above). Any such interaction will reduce as the scour depth increases and with it the value of h/D. The main parameter influencing variable-reversing scour appears to be U/U_c, as the amount of scour that occurs during the live-bed time-steps is greater than that during the transitional flow time-steps, which is much greater than that during the clear-water time-steps. This is not observed in the unidirectional test, where the constant U/U_c leads to the scour development exhibiting the typical curve observed in previous work (for example Melville and Coleman 2000). Here, when U/U_c is held constant, the time development is a smooth, asymptotic curve.

Scour Hole Shape

Figure 16 shows the final URS readings for the unidirectional test. The difference in scour hole shape is noticeable compared to Figure 12c; the downstream (B) side has a shallower slope than the upstream (A) side, indicating that the scour hole is elongated downstream. The scour hole is deeper in all measured directions as well as wider in the downstream (B) and lateral planes compared to Figure 12c. The mean final slope angles for each measurement plane for the unidirectional test are given in Table 3. For example, the mean slope of the 90˚ plane is the mean of the slope angles between transducers 4 - 5, and 5 – 6. Clearly, the tidal scour hole is significantly shallower than the unidirectional scour hole.

After one full cycle of variable reversing flows, the scour hole has developed sufficient depth for it to retain symmetry regardless of flow direction. This is contrary to Margheritini et al. (2006) who found that the scour hole continues to adjust in response to a reverse in current direction during the third and fourth half-cycles. The more realistic representation of tidal flow in the present experiments suggests that this asymmetry may not actually occur. These experiments include the transition and clear-water time-steps which both generate significantly less scour than the live-bed time-steps. This means that the scouring potential during each half-cycle of the tide is significantly less than it is in Margheritini et al. (2006), hence any change in scour hole morphology in response to the reversed flow will take longer. In these experiments, such changes take longer than a half-cycle. However, some of the experiments conducted by Margheritini et al. (2006) (tests 2.10 - 2.18) have similar flow conditions to the current tests. The velocity used was similar (U = 0.3m/s), water depth varied from 0.1 to 0.29m, median sediment grain size was d_{50} = 0.00015m and cylinder diameter was D = 0.2m. The length of a half tidal cycle was 30 minutes. This suggests that the incorporation of tidally-based variations in flow velocity and depth in the present experiments result in symmetrical scour hole development since neither flow direction dominates the morphological development of the scour.

Figure 10a shows that when the flow reverses, clear-water conditions in TS4 cause negligible further scour to occur. In itself, the clear-water flow intensity should be large enough to generate scour (as $U/U_c > 0.5$, Hoffmans and Verheij 1997). There are three possible reasons for no scour occurring here: 1) the scour hole generated by the previous transition and live-bed time-steps is already greater than the equilibrium scour depth for clear-water conditions; 2) the morphology of the scour hole has altered the flow near the cylinder, reducing its scouring potential; or 3) the rate of scour is slow in comparison to the length of the time-step. Considering (8), which predicts a scour depth of 0.95D for the clear-water conditions, and the fact that the previous clear-water time step did generate scour, the second and third points above give the most likely explanation for negligible scour during TS4.

While there is minimal change in the depth and scour hole orientation during TS4, once TS5 begins, the scour hole orientation adjusts to the new flow direction. The upstream side becomes deeper and the downstream side, due to the low intensity of the wake, is filled in close to the cylinder before scour continues and the depth increases (Figure 10a and b). Deposition does not occur during the reversal in TS7, likely because the transitional flow is turbulent enough to keep sediment in suspension for longer, allowing it to be transported out of the scour hole. The adjustment of the scour hole to the new flow direction occurs relatively quickly, after a delay of approximately 5 minutes (Figure 11a).

The scour hole at the end of the two full tidal cycles is more symmetrical than was found under unidirectional flow conditions. The finding that scour development in the variable reversing test take longer needs validation through further tests. Such tests should be run to equilibrium. This would allow more accurate extrapolation to prototype conditions.

The rates of scour predicted by some of the widely-used equations for unidirectional flow are different from those measured here, mainly due to problems of estimation of the time-scale needed for the development of the equilibrium depth. As the flow conditions change over each tidal cycle, so does the rate of scour (or infilling), and this is not accounted for in the equations considered above.

Conclusions

This paper presents results of an experimental investigation into the development of scour under variable reversing currents. The scaled tide was divided into half-cycles, each of which was resolved into three time-steps in which flow speed and depth were constant. At the end of each half-cycle the flow direction was reversed and a symmetric second half-cycle began. The test ran for a total of four half-cycles.

The rate of scour was found to change over each half cycle, as the flow regime varied from live-bed to transitional to clear-water regimes and *vice versa* under the reversed flow condition. During the first half-cycle, the scour hole shape was analogous to that generated by a unidirectional current. In the second half cycle, the reversal of current direction both delayed the continuation of scour and caused the scour hole to become more symmetrical. This symmetry persisted throughout the remainder of the test. Changes in scour depth and shape in the third half-cycle were significantly smaller. The fourth half-cycle had little effect, with the hole maintaining a symmetrical shape and the scour depth stabilising.

Overall, the equilibrium scour depth found in the variable reversing current conditions used in this test was lower than that predicted by existing equations (which are derived from unidirectional current measurements) or measured in ‘square-tide’ experiments. Thus, extrapolating these findings to prototype scale suggests that the amount of scour protection required and therefore the costs of scour protection could be reduced. Despite the special care taken in design of the experiment to present plausible field conditions and fulfil the scaling laws for flow properties and sediment transport, the simplifications made in the experiment as well as laboratory effects would affect the scour hole shape, depth and time development. Hence it would not be appropriate to derive practical guidelines solely on the data of this experiment. The key finding from these experiments is that they demonstrate that changing flow direction and intensity will affect the final scour hole depth and its time-development. Furthermore, these data can be used for validation of the numerical models which can then be applied to test different prototype flow conditions. Future experiments should consider a constantly changing tidal current depth, speed and direction as well

as the case of combined wave and current action on the scour development.

Acknowledgements

This work was fully funded by the Supergen Wind Energy Technology EPSRC grant.

Time Step	Flow Direction	Upstream Plane	Test Condition	Tidal Stage	Tidal Half-Cylcle	Duration [mins]	U [m s^{-1}]	h [m]	U/U_c	θ	h/D	Re_D	Fr
Unidirectional Scour Test													
-	Unidirectional	A	Live-bed	mid-tide	-	162	0.31	0.25	1.24	0.1	1.25	7.9×10^4	0.22
Variable Reversing Current Scour test													
1	Positive	A	Transition	low-tide	1st	27	0.23	0.1	1.02	0.044	0.5	2.3×10^4	0.23
2	Positive	A	Live-bed	mid-tide	1st	27	0.31	0.2	1.24	0.11	1	6.3×10^4	0.22
3	Positive	A	Clear-water	high-tide	1st	27	0.15	0.4	0.54	0.041	2	6.1×10^4	0.08
4	Negative	B	Clear-water	high-tide	2nd	27	0.15	0.4	0.54	0.041	2	6.1×10^4	0.08
5	Negative	B	Live-bed	mid-tide	2nd	27	0.31	0.2	1.24	0.11	1	6.3×10^4	0.22
6	Negative	B	Transition	low-tide	2nd	27	0.23	0.1	1.02	0.044	0.5	2.3×10^4	0.23
7	Positive	A	Transition	low-tide	3rd	27	0.23	0.1	1.02	0.044	0.5	2.3×10^4	0.23
8	Positive	A	Live-bed	mid-tide	3rd	27	0.31	0.2	1.24	0.11	1	6.3×10^4	0.22
9	Positive	A	Clear-water	high-tide	3rd	27	0.15	0.4	0.54	0.041	2	6.1×10^4	0.08
10	Negative	B	Clear-water	high-tide	4th	27	0.15	0.4	0.54	0.041	2	6.1×10^4	0.08
11	Negative	B	Live-bed	mid-tide	4th	27	0.31	0.2	1.24	0.11	1	6.3×10^4	0.22
12	Negative	B	Transition	low-tide	4th	27	0.23	0.1	1.02	0.044	0.5	2.3×10^4	0.23

Table 1

Probe	Plane	Variable Reversing Test end of first cycle (t = 162 min). d_{sc}/D	End of Variable Reversing Test. d_{sc}/D	Unidirectional Test. d_{sc}/D
1	A	0.405	0.495	0.6
4	B	0.48	0.5	0.7
7	90	0.38	0.5	0.6
10	270	0.45	0.55	0.65

Table 2

Measurement Plane	Unidirectional Mean Slope Angle [degrees]	Tidal Mean Slope Angle [degrees]
A	28.9	11
B	25.5	11.2
90	29.7	11.4
270	28.2	11.8

Table 3

References

Breusers, H. N. C., Nicollet, G., and Shen, H. W. (1977). "Local Scour around Cylindrical Piers." *Journal of Hydraulic Research,* 15**,** 211-252.

Breusers, H. N. C., and Raudkivi, A. J. (1991). "Scouring." Balkema, Rotterdam.

De Vos, L. (2008). "Optimisation of Scour Protection Design for Monopiles and Quantification of Wave Run-Up: Engineering the Influence of an Offshore Wind Turbine on Local Flow Conditions." Ph.D. Thesis, Universiteit Gent. Faculteit Ingenieursweten-schappen. Ghent, Belgium.

Escarameia, M., May, R. W. P. (1999). "Scour around Structures in Tidal Flows." *Report SR 521,* HR Wallingford Group Ltd, Wallingford, U.K.

Ettema, R., (1980). Scour at Bridge Piers. *Report No.* 216, University of Auckland, Auckalnd, New Zealand.

Ettema, R., Melville, B. W., and Barkdoll, B. (1998). "Scale Effect in Pier-Scour Experiments." *Journal of Hydraulic Engineering*, 124**,** 639 - 642.

HEC-18. (1993). "Evaluating Scour at Bridges." *US Department of Transportation, Report No FHwA-IP-90-017*. Federal Highway Administration (FHwa), Washington, D.C.

Hoffmans, G. J., and Verheij, H.G. (1997). "Scour Manual." Balkema, Rotterdam, The Netherlands.

Hughes, S. A. (1993). "Physical Models and Laboratory Techniques in Coastal Engineering." *Advanced Series on Ocean Engineering*. Vol. 7. World Scientific, Singapore.

Jensen, M. S., Larsen, B. J., De Vos, L., Christiansen, E. D., Hansen, E, A., Solberg, T., Hjertager, B. H., and Bove, S. (2006). "Offshore Wind Turbines Situated in Areas with Strong Currents." M. S. Jensen, ed., Esbjerg, Offshore Centre Denmark.

Johnson, A. (1995). "Comparison of Pier-Scour Equations Using Field Data." *Journal of Hydraulic Engineering*, 121**,** 626 - 629.

Kim, S.-C., Friedrichs, C. T., Maa, J. P.-Y., and Wright, L. D., (2000) "Estimating Bottom Stress in Tidal Boundary Layer from Acoustic Doppler Velocimeter Data." *Journal of Hydraulic Engineering*, 126**,** 399-406.

Margheritini, L., Martinelli, L., Lamberti, A., and Frigaard, P. (2006). "Scour around Monopile Foundation for Offshore Wind Turbine in the Presence of Steady and Tidal Currents." *Proceedings of the International Conference on Coastal Engineering*. ICCE San Diego, California, USA. 2330-2342.

McGovern, D., Ilic, S., McClelland, S., Folkard, A., Murphy, B. (2009). "Turbulence and Shear Stress Around Offshore Wind Turbine Pile in Tidal Currents Using Particle Image Velocimetry." *Proceedings of Coastal Dynamics*. Kajima Sci Fdn, Tokyo, Japan.

McGovern, D. J. (2011). "The Interaction of Tidal Currents with Offshore Wind Turbine Monopiles: an Experimental Study of Flow, Turbulence, Scour and the Reduction of Scour around the Monopile." Ph.D Thesis, Lancaster University, Lancaster, U.K.

Melville, B. W. (1975). "Local Scour at Bridge Sites." Ph.D Thesis, School of Engineering, Auckland University, Auckland, New Zealand.

Melville, B. W., and Sutherland, A. J. (1988). "Design Method for Local Scour at Bridge Piers." *Journal of Hydraulic Engineering*, 114**,** 1210 - 1226.

Melville, B. W. (1997). “Pier and Abutment Scour - an Intergrated Approach.” *Journal of Hydraulic Engineering*, 123**,** 125-136.

Melville, B. W., and Chiew, Y. M. (1999). “Time Scale for local Scour at Bridge Piers.” *Journal of Hydraulic Engineering*, 125**,** 59-65.

Melville, B. W., and Coleman, S. E. (2000) “Bridge Scour.” Water Resources Publications, Colorado, USA.

Raudkivi, A. J., and Sutherland, A. J. (1981). “Scour at Bridge Crossings.” *Road Resources Unit Bulletin 54*, Wellington, New Zealand.

Roulund, A., Sumer, B. M., Fredsøe, J., and Michelsen, J. (2005). “Numerical and experimental Investigation of flow and Scour around a Circular Pile. *Journal of fluid Mechanics*, 534, 351-401.

Shen, H. W., Schneider, V. R., and Karaki, S. S. (1969). “Local Scour Around Bridge Piers.” *Journal of the Hydraulics Division*. ASCE, 95**,** 1919 - 1940.

Sheppard, M. D., Odeh, M., and Glasser, T. (2004). “Large Scale Clear-Water Local Pier Scour Experiments.” *Journal of Hydraulic Engineering*, 130**,** 957-963.

Soulsby, R. L. (1986). “Coastal and Estuarine Sediment Dynamics.” In: Dyer, R. K. (Ed.) *Coastal and Estuarine Sediment Dynamics* New York, Wiley-Interscience.

Sumer, B. M., Christiansen, N., and Fredsøe, J. (1992). “Time Scale of Scour around Vertical Pile.” *2nd International Offshore and Polar Engineering Conference. The International Society of Offshore and Polar Engineers*. San Fransisco, CA, USA.

Sumer, B. M., Fredsøe, J., and Christiansen, N. (1992a). “Scour around Vertical Pile in Waves.” *Journal of Waterway, Port, Coastal, and Ocean Engineering*, 117, 15 - 31.

Sumer, B. M., and Fredsøe, J. (1997). “Hydrodynamics around Cylindrical Structures.” World Scientific. Singapore.

Sumer, B. M., and Fredsøe, J. (1999). “Wave Scour around Structures.” *Advanced Series on Ocean Engineering*, World Scientific, Singapore.

Sumer, B. M., and Fredsøe, J. (2001). “Scour around a Pile in Combined Waves and Current.” *Journal of Hydraulic Engineering*, 127**,** 403 - 411.

Sumer, B. M., Christiansen, N., and Fredsøe, J. (1997). “Horseshoe Vortex and Vortex Shedding around a Vertical Wall-mounted Cylinder Exposed to Waves.” *Journal of Fluid Mechanics*, 332**,** 41-70.

Whitehouse, R. J. S. (1998). “Scour at Marine Structures.” Thomas Telford, London, UK.

Wilson, J. C., Elliot, M., Cutts, N. D., Mander, L., Mendao, V., Perez-Dominguez, R., and Phelps, A. (2010). “Coastal and Offshore Wind energy Generation: Is It Environmentally Benign?” *Energies*, 3(7), 1383-1422.

Zaaijer, M. B., and Van Der Tempel, J. (2004). “Scour Protection: a Necessity or a Waste of Money?” *43rd IEA Topical Expert Meeting - Critical Issues Regarding Offshore Technology and Deployment*. Skaerbaek, Denmark.

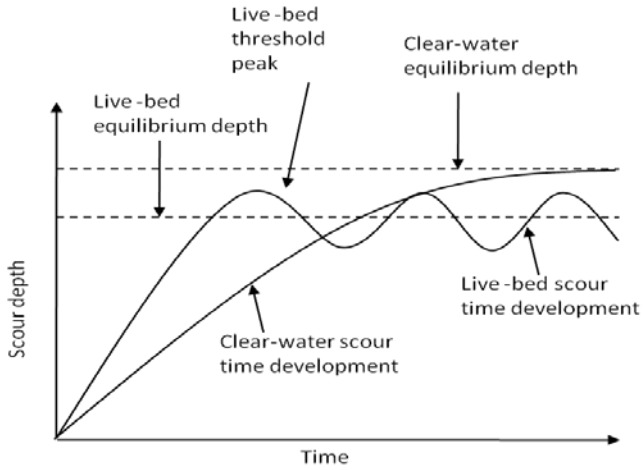

Figure 1

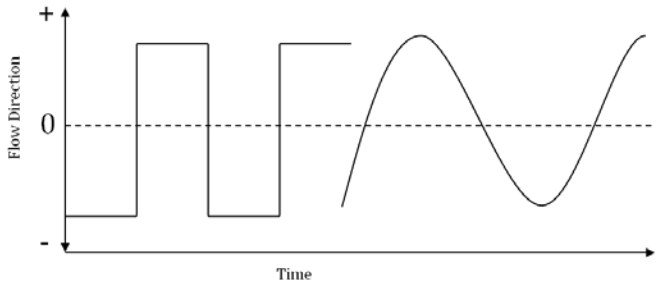

Figure 2

Figure 3

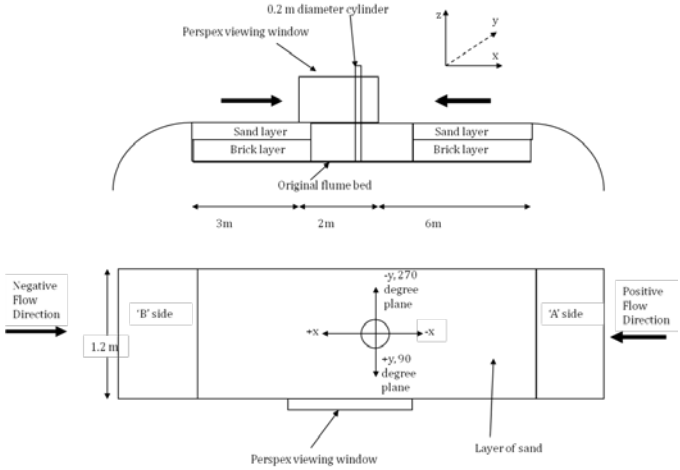

Figure 4

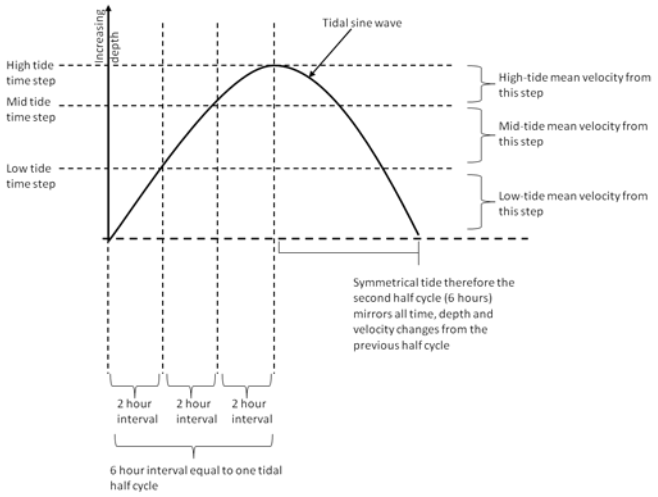

Figure 5

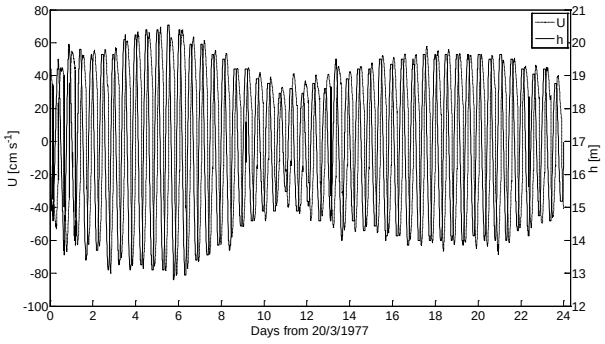

Figure 6

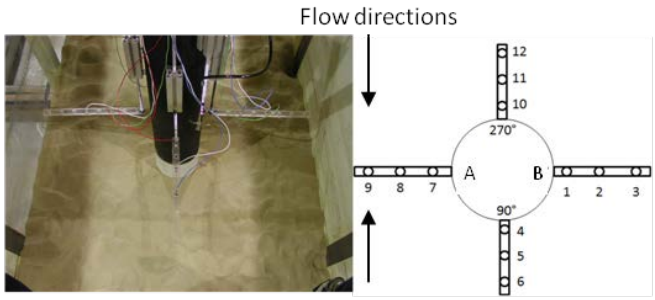

Figure 7

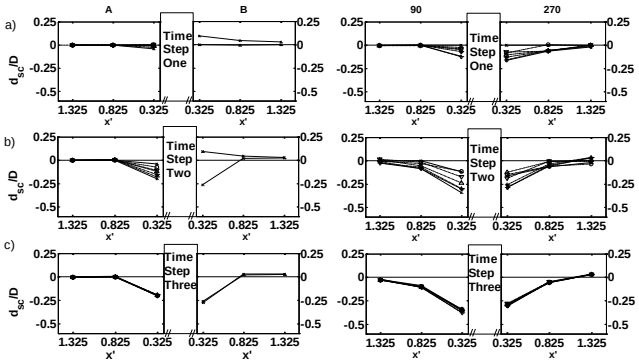

Figure 8

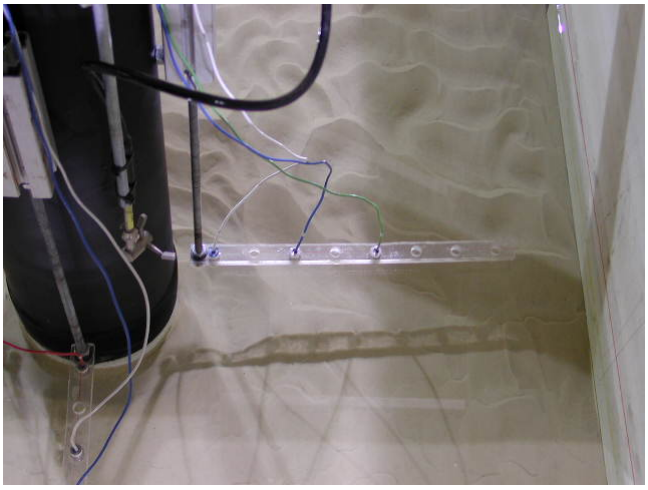

Figure 9

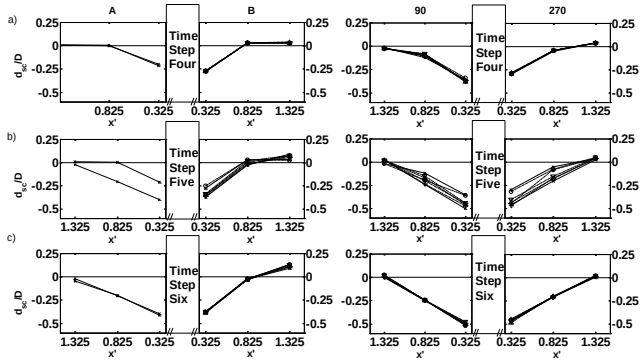

Figure 10

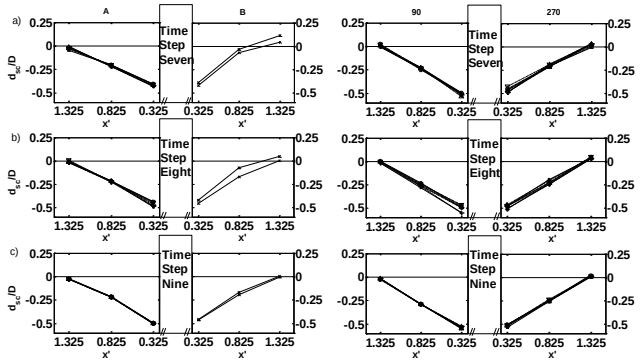

Figure 11

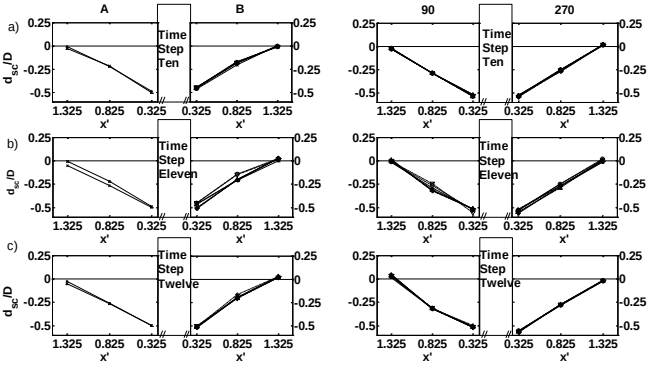

Figure 12

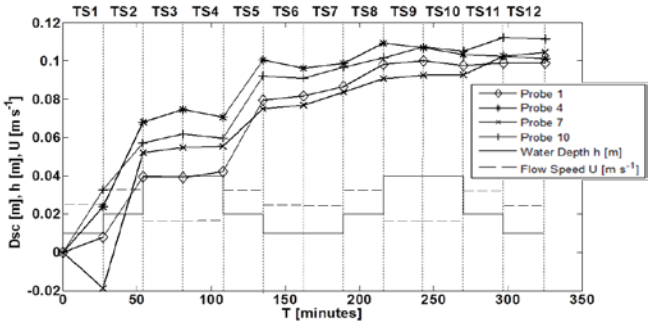

Figure 13

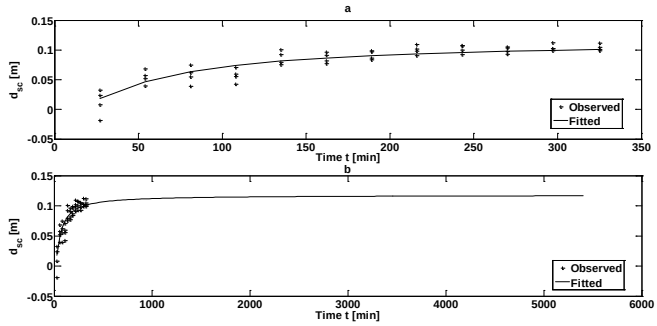

Figure 14

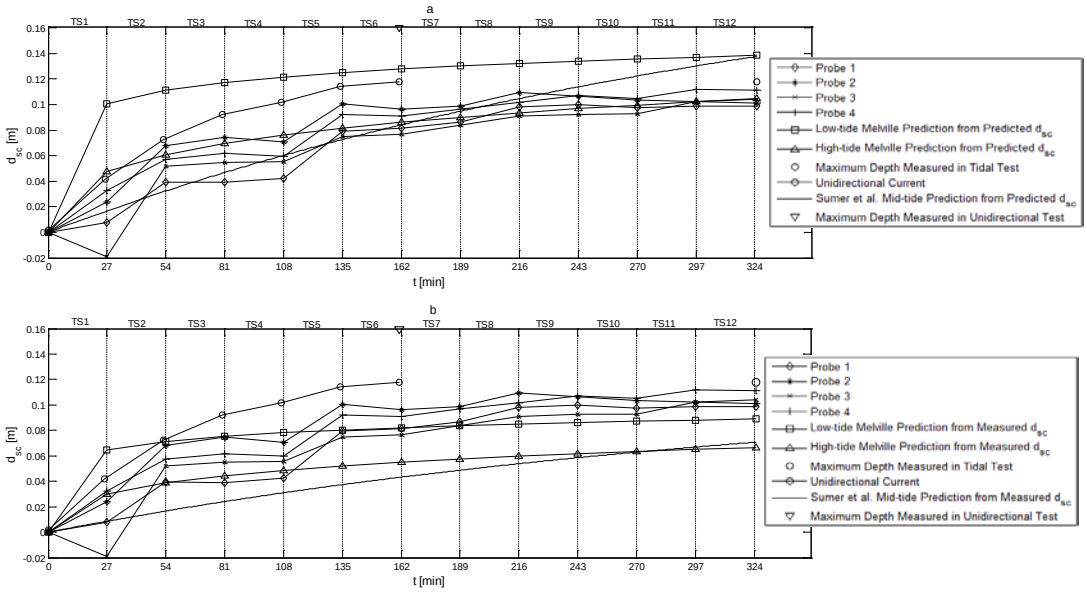

Figure 15

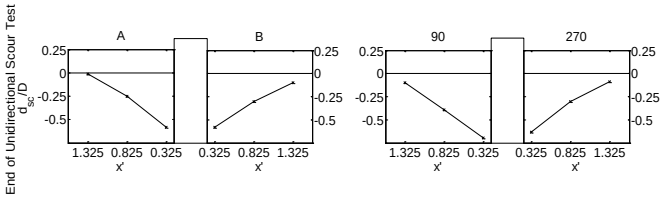

Figure 16

Figure Captions

Figure 1. Comparison of the time development of clear-water and live-bed scour, after Breusers and Raudkivi (1991).

Figure 2. Square tide where velocity is equal and opposite for each half-cycle (left), and a sinusoidal tide (right).

Figure 3. Image of the flume constructed within the tank with the test cylinder positioned at the midpoint of the flume.

Figure 4. A schematic diagram of the flume set-up.

Figure 5. Schematic diagram showing the construction of the test time-step from the sinusoidal non-progressive tide.

Figure 6. Sample flow speed and depth time series from a tidal gauge and current meter in Liverpool Bay, U.K. Data name b0015569, and collection date 1977.

Figure 7a-b. An image of the URS deployment around the cylinder, (7a) a schematic diagram of the URS positions with the origin is set at the cylinder centre (7b).

Figure 8a-c. URS time series scour development between TS1 (8a), TS2 (8b), and TS3 (8c). Depth at the start of each time-step is denoted by crosses on a medium weight black line, and at the end of the time-step by crosses on a heavy black line. Time-series depth readings at 5, 10, 15, 20 and 25 minutes are represented by the circles, down-triangles, up-triangles, stars, and plus signs respectively on dashed lines for each plane except the downstream (B) plane, which shows only the start and end readings. The edges of the cylinder are located at their true positions along the adjacent x axes; that is, at $x' = 0$. However, the cylinder diameter is not scaled to the adjacent x axes (as denoted by axis break symbols).

Figure 9. Rippling of the bed after time-step two.

Figure 10a-c. URS time series scour development between TS4-6. Symbols as in Figure 7a-c.

Figure 11a-c. URS time series scour development between TS7 to 9. Symbols as in Figure7-c.

Figure 12a-c. URS time series scour development between TS10-12. Symbols as in Figure 7a-c.

Figure 13. Variable reversing scour time-development for the closest probes to the cylinder at each radial position (top), water depth and current speed (bottom).

Figure 14. Exponential curve fitted to the data from probes 1, 4, 7 and 10 (top), and the extrapolation of the curve to 90 hours (bottom). The fit is strongly statistically significant ($r^2 = 0.7$; $df = 46$; $p < 0.001$).

Figure 15a-b. a) Time-development of scour at URS probes 1, 4, 7 and 10 with the curve for the

transition and clear-water time-step predicted using the Melville and Chiew (1999) method and the live-bed time-step predicted using the Sumer et al. (1992a) curve (1-2 and 3-4 respectively). d_{sc} is calculated from Equation (5). Also plot is the maximum depth measured in the unidirectional test (down triangle) and variable reversing test (circle); both measured using the laser profiler at $x' = 0.75$ and $y' = 0.5$. b) As in Figure 13a except d_{sc} is taken as from the measured variable reversing maximum (Table 3). Note the less-smooth development of scour recorded by the URS probes in comparison to all prediction curves.

Figure 16. Final URS scour depth reading for the unidirectional scour hole. Symbols as in Figure 8a-c.

Table Captions

Table 1. Test conditions.

Table 2. The final measured values of d_{sc}/D at probes 1, 4, 7 and 10 for the variable reversing and unidirectional tests.

Table 3. The mean slope angles for each measurement plane at the end of the unidirectional and tidal tests.